ACS APPLIED NANO MATERIALS

www.acsanm.org Article

Spectrally Tunable White Light-Emitting Diodes Based on Carbon Quantum Dot-Doped Poly(*N*-vinylcarbazole) Composites

Kevser Sahin Tiras, Aysenur Biçer, Ehsan Soheyli,* and Evren Mutlugun*

Cite This: *ACS Appl. Nano Mater.* 2024, 7, 2744−2752 Read Online

ACCESS | Metrics & More | Article Recommendations | Supporting Information

ABSTRACT: Electroluminescent white light-emitting diodes (WLEDs) are always of great interest for emerging display applications. Carbon-based quantum dots (CQDs) are the newest emerging nanoscale materials that can be employed for this purpose, owing to their broad and bright light emission properties. In the present work, highly luminescent CQDs with an emission quantum yield of 60% were prepared via a colloidal solvothermal method and subsequent silica gel column chromatography. The photoluminescence (PL) peak was located at 550 nm possessing yellow emission, with a full width at half-maximum of 98 nm and a relatively long lifetime of 10.23 ns through a single-exponential recombination pathway. CQDs were employed in an electroluminescent device architecture of an ITO/PEDOT:PSS/TFB/CQD:PVK/TPBi/LiF/Al structure and blended with poly(*N*-vinylcarbazole) (PVK) to evaluate their ability to reach white electroluminescent emission. Results confirmed a high external quantum efficiency (EQE) of 0.76% and a maximum luminescence of 774.3 cd·m^{-2}. Tuning the ratio between CQDs and PVK from 1:10.25 to 1:5.75 resulted in a systematic shift in CIE $x-y$ coordinates from 0.23−0.26 to 0.21−0.24, located close to the cool white region. The results of the present study can be considered a step forward in fabricating efficient WLEDs based on low-cost CQDs.

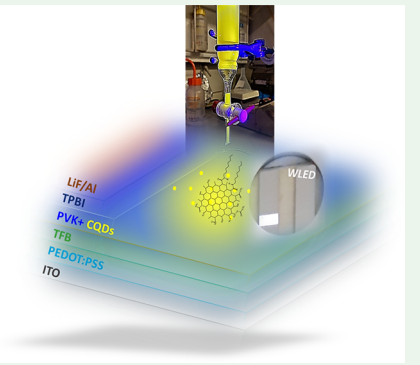

KEYWORDS: *solvothermal, carbon quantum dots, yellow emission, high quantum efficiency, electroluminescence, white light-emitting diodes*

1. INTRODUCTION

Carbon-based quantum dots (CQDs) are an attractive member of luminescent nanoscale materials with unique benefits for a wide range of applications.[1,2] Representing a set of extremely demanding advantages in chemistry (a simple, low-cost, and scalable synthesis method), biology (earth-abundant and biofriendly precursors), and physics (unique optical and structural properties) has made CQDs capable of being used in diverse applications of sensing,[3] biomedicine,[4,5] optoelectronics,[6] and sunlight harvesting.[7,8] One of the highly demanding aspects is the ability for electroluminescent technology and light-display panels to be progressively updated to reach industrial requirements. This is even more interesting for the direct fabrication of electroluminescent white light-emitting diodes (WLEDs) due to the intrinsic wide photoluminescence (PL) profile of the CQDs that is rarely observed in other well-known luminescent quantum dots (QDs).

Recently, various attempts have been dedicated to preparing luminescent CQDs for white light-emitting panels, and almost in all of them, the solvothermal/hydrothermal method is the one employed to fulfill the necessities of preparing high-quality samples with the possibility of mass production.[9,10] Apart from the ability to afford high-quality CQDs, this method does not require harsh and specific reaction mediums and instruments. Besides, it can be easily upgraded to the upscale level for the industry where current research has tried to converge. Nonetheless, it produces high concentrations of unreacted species and impurities, which have to be removed via several post-treatment procedures such as column chromatography, dialysis, etc.

From the electronic perspective, CQDs usually show a large Stock shift and a broad spectrum of emitted photons that satisfy the requirement to reach the white emission region in the Commission Internationale de L'Eclairage (CIE) chromaticity coordinate. In general, this can be fulfilled by either color conversion or direct white electroluminescence. Wei et al. used hydrothermally synthesized multicolor CQDs for the fabrication of color-converted white emission.[11] Zhou's group proposed a simple one-pot solvothermal method, followed by column chromatography, to synthesize uniformly monodispersed CQDs with PL peaks located at 435, 495, 525, and 595 nm.[12] The highest photoluminescence quantum yield (PLQY) was about 89% and full width at half-maximum (FWHM) was

Received: October 15, 2023
Revised: December 7, 2023
Accepted: January 3, 2024
Published: January 26, 2024

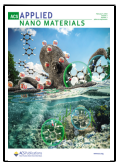

https://doi.org/10.1021/acsanm.3c04915
ACS Appl. Nano Mater. 2024, 7, 2744−2752

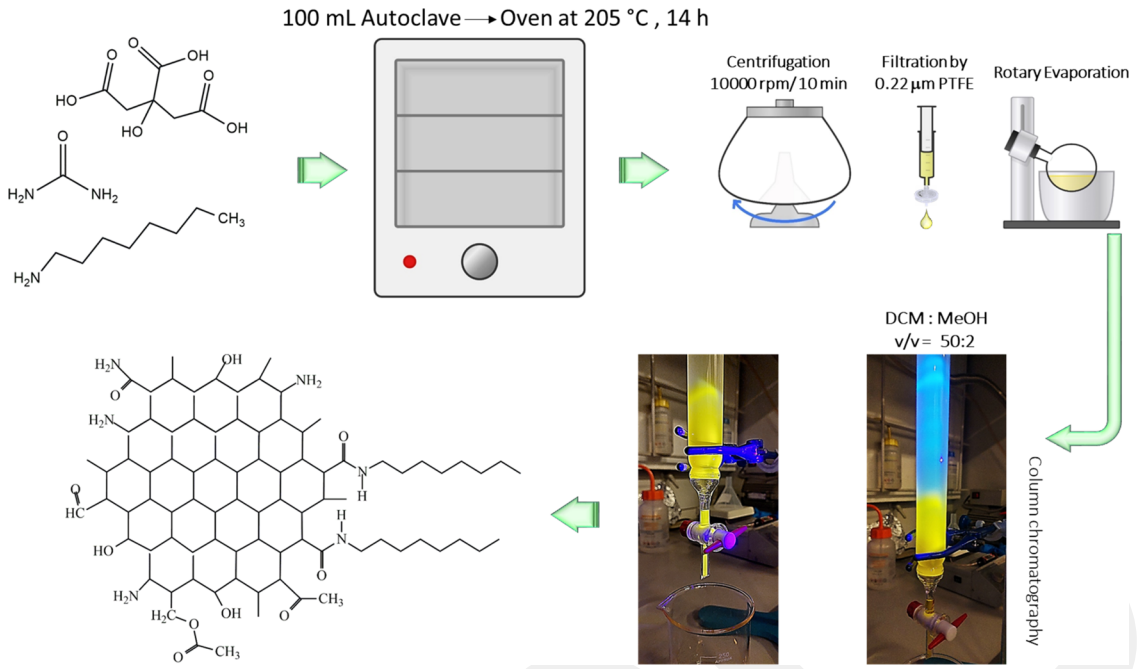

Figure 1. Schematic of the synthesis method and structure of CQDs.

as narrow as 31 nm. They confirmed the capability of the fabrication of a CQD-based color-converted WLED with a high color rendering index (CRI) of 90.8, a low correlated color temperature (CCT) of 4534 K, and a CIE coordinate of (0.361, 0.369). However, the fabrication of an electroluminescent WLED is more demanding and challenging from a technological point of view. This can be accomplished either via employing CQDs as a single emissive layer or blending them into organic agents like poly(*N*-vinylcarbazole) (PVK).[13] CQDs usually suffer from quenched luminescence in the solid-state form,[14] resulting in a reduced luminance for CQD-LED.[15] Doping CQDs in poly(*N*-vinylcarbazole) (PVK) is one way to improve the low luminance of the device to reach a desired blue, green, or red emission or to produce a white emission.[16,17] A designed solvothermal method was proposed using suitable carbon and nitrogen sources to prepare bright multicolor-emitting CQDs.[16] They fabricated tunable electroluminescence across the visible spectrum, along with a WLED using green CQD-blended PVK as an emissive layer. The WLEDs showed a CIE coordinate at (0.30, 0.33) with the L_{max} and η_c up to 2050 cd·m^{-2} and 1.1 cd·A^{-1}, respectively, at a low turn-on voltage of 3.9 V. Wang et al. engineered the reactants and their molar ratio to synthesize bright and tunable CQDs with the fabrication possibility of various high-CRI (warm, standard, and cold) WLEDs.[18]

Here, organically soluble N-doped CQDs with a peak emission centered at 550 nm and a monoexponential recombination pathway were synthesized using the solvothermal method. The purified CQDs showed dual features of a high PLQY of 60% and a very broad PL spectrum, which support the possibility of the direct fabrication of WLEDs. As a proof of concept, white light electroluminescent CQD-LEDs were fabricated by using a host−guest blend as an emissive layer, wherein yellow-emissive CQDs played the role of the guest and PVK was used as the host. The electrical measurements carried out for the fabricated WLEDs confirmed a relatively high external quantum efficiency (EQE) of 0.76% with proper CIE coordinates in the white emission region. Tuning the CQD/PVK volume ratio, a desired systematic shift in CIE coordinates in the cool white region was achieved, demonstrating an engineered white light.

2. EXPERIMENTAL SECTION

2.1. Materials. Citric acid (99.5−100.5%, Merck), n-octylamine (99.0%, Aldrich), urea (BioXtra, Sigma-Aldrich), toluene (EMPLURA, Merck), dichloromethane (DCM) (EMSURE, Merck), methanol (≥99.7%, Tekkim), chloroform (EMSURE, Merck), silica gel 60 (0.040−0.063 mm, Merck), indium tin oxide (ITO) (Ossila, S101), PEDOT:PSS (poly(3,4-ethylene dioxythiophene):poly(styrene-sulfonate), AI 4083), PVK (poly(9-vinylcarbazole), Aldrich), poly[(9,9-dioctylfluorenyl-2,7-diyl)-*co*-4,4′-(*N*-(4-s-butyl phenyl)-diphenylamine)] (TFB, Lumtec, M_w = 10,000−30,000), 2,2′,2″-(1,3,5-benzinetriyl)-*tris*(1-phenyl-1-*H*-benzimidazole) (TPBi, Sigma-Aldrich, ≥99.5%), and lithium fluoride (LiF, Sigma-Aldrich, ≥99.99%) were used as received for the synthesis of CQDs and fabrication of LEDs.

2.2. Synthesis Method. A solvothermal method was used for the preparation of high-quality CQDs. One mmol of citric acid and 0.5 mmol of urea were added into 30 mL of toluene and heated at 40 °C for a short time. Then, 0.5 mmol of *n*-octylamine was added into the mixture, which was again stirred for a while. After that, the solution was transferred to a 100 mL Teflon-lined autoclave and reacted at 205 °C for 14 h. Finally, the reactor was put outside of the oven and left to cool down naturally. To purify the colloidal product, the as-prepared colloidal CQDs were first centrifuged at 10,000 rpm for 10 min to discard the unreacted species and then filtered by a 0.22 μm poly(tetrafluoroethylene) (PTFE) filter. In the next step, using silica gel column chromatography as a stable phase and DCM/methanol as an eluent mobile phase, purified CQDs with strong yellow emission were separated. In the end, it was concentrated via a rotary evaporator and redispersed in DCM for further experiments and device fabrication. A schematic illustration of the synthesis method and the possible structure of CQDs based on Fourier transform infrared (FTIR) spectroscopy and X-ray photoelectron spectroscopy (XPS) has been drawn and is shown in Figure 1.

2.3. CQD-LED Fabrication. Glass substrates prepatterned with indium tin oxide (ITO) were cleaned in an ultrasonic cleaner to remove impurities by using a 0.1% volume ratio Hellmanex:hot DI water mixture, hot DI water, and isopropanol alcohol, followed by

https://doi.org/10.1021/acsanm.3c04915
ACS Appl. Nano Mater. 2024, 7, 2744−2752

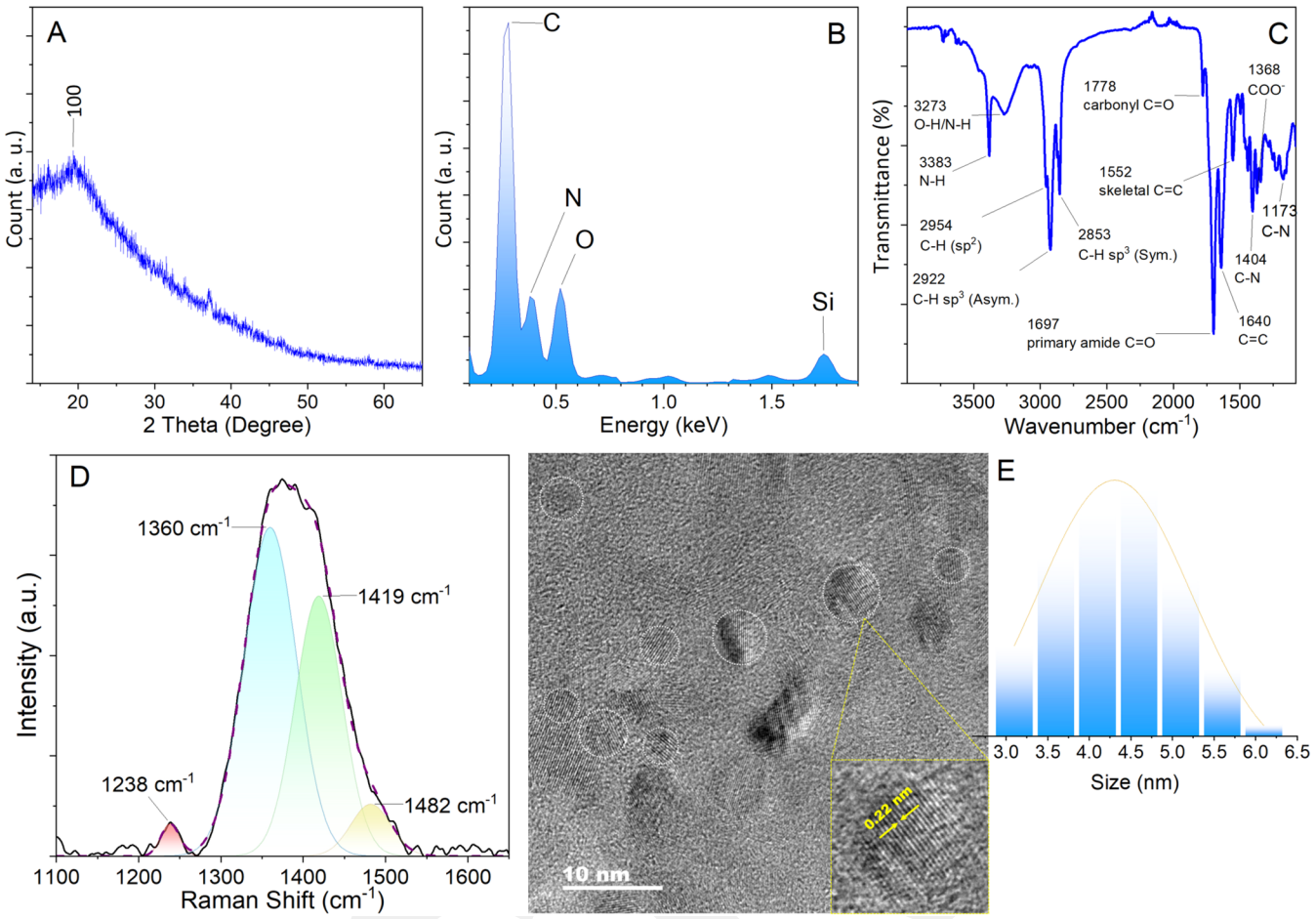

Figure 2. (A) XRD pattern, (B) STEM-based EDX profile, (C) ATR-FTIR spectrum, (D) baseline-corrected Raman spectrum, and (E) TEM image of the purified CQDs and its corresponding size histogram. The inset shows magnified CQDs with a 0.22 nm interplanar distance.

plasma cleaning. As the hole injection layer, PEDOT:PSS was spin-coated on ITO at 5000 rpm for 60 s and then annealed at 150 °C for 20 min. After annealing, substrates were transferred into the argon-filled glovebox. Then, an 8 mg/mL chlorobenzene solution of TFB was spin-coated on the PEDOT:PSS layer at 3000 rpm for 60 s and annealed at 150 °C for 30 min. CQDs (15 mg/mL in DCM) were doped in 6 mg/mL PVK solution in chloroform. The blends were prepared in different volume ratios of CQDs and PVK to use as an emissive layer. By keeping the total volume of all of the blends the same, only CQD:PVK volume ratios changed, and the ratios followed as 1:5.75, 1:7.25, 1:8.75, and 1:10.25. CQD-PVK solutions were spin-coated on TFB at 2000 rpm for 60 s and annealed at 60 °C for 15 min. The cathode layer consisting of LiF (1 nm) and Al (100 nm) was deposited by thermal evaporation at a base pressure of 5×10^{-6} Torr on top of the thermally evaporated 70 nm of electron transport layer TPBi. Finally, to protect the device from oxidation and humidity, the active area of the device was encapsulated with ultraviolet (UV)-curable epoxy and encapsulation glass.

2.4. Characterizations. The X-ray diffraction (XRD) pattern was collected via a Bruker D8 Discover diffractometer. Attenuated total reflectance (ATR) Fourier transform infrared (FTIR) spectroscopy known as ATR-FTIR was performed using the FTIR spectroscopy model NICOLET 6700 made by Thermo Scientific. A Raman microscopy system (WITec α M+) with laser excitation of 785 nm under 20 μW power using a 50× (NA:0.80) objective and an integration time of 2 s was used. The X-ray photoelectron emission spectrum (XPS) was acquired via a Thermo Scientific K α X-ray spectrometer. A Hitachi HF5000 coldFEG Cs corrected scanning transmission electron microscope equipped with a Gatan OneView camera and an Oxford Instruments XMax-100 energy-dispersive X-ray (EDX) detector was used at an operating voltage of 200 kV to capture a transmission electron microscopy (TEM) image. The optical spectroscopies were performed via UV-visible (UV−vis), PL/PL excitation (PLE), and time-resolved PL (TRPL) spectroscopies and via measurement of the PLQY. Data were recorded using a Thermo Genesys 10S spectrometer, a Cary Eclipse, PicoQuant Fluo Time 200 time-correlated single photon counting system (TCSPC), and a Quantaurus-QY instrument made by Hamamatsu Company, respectively. A Hamamatsu PMA-12 photonic multichannel analyzer and a Keithley 2400 source meter together with an integrating sphere were used for characterization. The luminance, EL, and color coordinate values of the devices were tested with these instruments.

3. RESULTS AND DISCUSSION

A set of experiments were conducted to verify the structure of the prepared CQDs. Despite the common luminescent QDs, the crystallinity of the carbon-based QDs is not usually strong, showing a graphite-like core and amorphous carbonates.[2] This has been demonstrated in Figure 2A, in which a very broad pattern related to the (100) crystalline planes of the hexagonal structure is observed, attributed to the short-range order of purified CQDs. The elements contributing to the CQDs were identified using STEM-based EDX analysis (Figure 2B), showing the presence of carbon and oxygen as main constituents and a few amounts of nitrogen due to the presence of urea. The Si and Au signals are related to the Si substrate and the coated layer of gold used for analysis. Since CQDs are shown as molecular-based electronic structures and

https://doi.org/10.1021/acsanm.3c04915
ACS Appl. Nano Mater. 2024, 7, 2744−2752

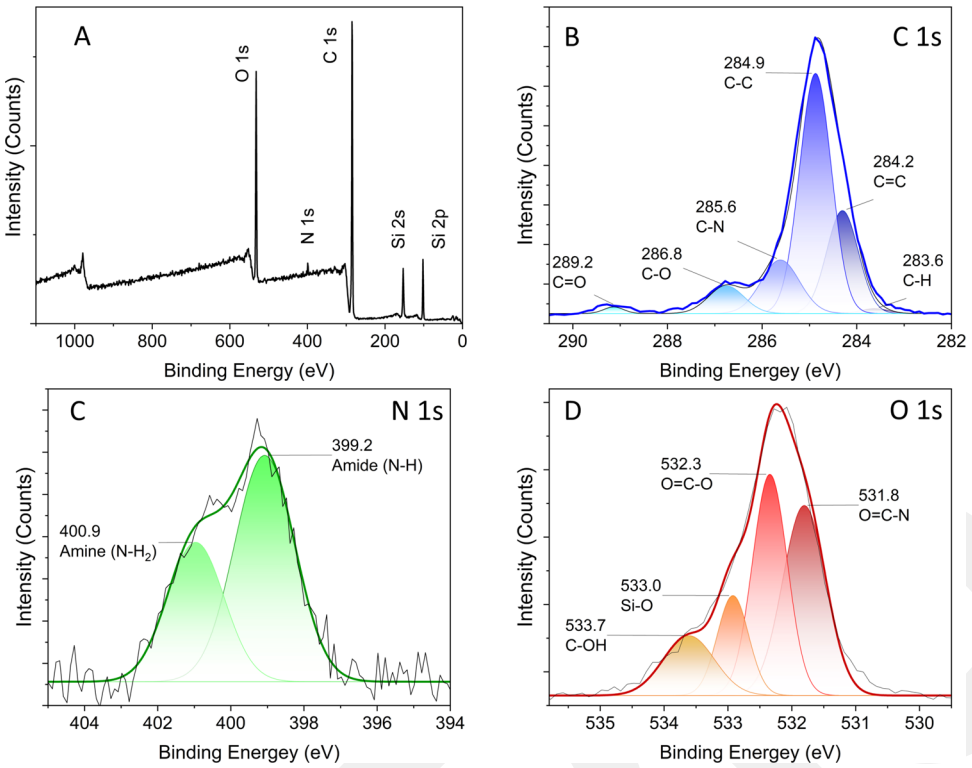

Figure 3. (A) XPS profile and deconvoluted high-resolution XPS results of purified CQDs for (B) carbon, (C) nitrogen, and (D) oxygen.

more importantly, a surface enriched with activated functional groups, performing IR spectroscopy is always beneficial. As shown in Figure 2C, the ATR-FTIR spectrum of the finalized sample contains a multiband pattern with distinctive signals. The stretching vibrations of sp^3 N−H secondary amine groups appeared at 3383 cm^{-1} referring to the successful reaction of the NH terminal of octylamine with carbonyl/carboxyl groups at the surface of CQDs. A relatively broad band at 3273−2380 cm^{-1} is related to the OH/N/H stretching signals. A very weak peak at 2954 cm^{-1} is assigned to the aromatic ring of sp^2 (C−H).[19] Intense signals at 2853 and 2922 cm^{-1} are related to the symmetric and asymmetric stretching sp^3 (C−H), respectively. These two peaks are stronger than those in other reports who just have used citric acid and urea.[20,21] Therefore, we can attribute this to the presence of a secondary amide of the octylamine carbonic chain. The intense band at around 1697 cm^{-1} reflects stretching vibrations of C═O amide, while C═O carbonyl functional groups have been located at 1778 cm^{-1}. The vibrations of C═C (skeletal) groups were also located at around 1552 and 1640 cm^{-1}.[8,22] The peak at 1404 cm^{-1} is related to the stretching vibrations of C−N,[23] while the one located at 1173 cm^{-1} is related to the bending vibrations. Finally, multiple peaks at around 1300−1368 cm^{-1} are attributed to the COO^- vibrational groups. All of these data confirmed the preparation of CQDs with the dominant presence of COOH, OH (hydroxyl), $CONH_2$ (amine), and CONH (amide) functional groups on the surface. The Gaussian-fitted Raman spectrum of the purified CQDs is plotted in Figure 2D. A tiny peak at around 1238 cm^{-1} can be assigned to the stretching vibrations of sp^2−sp^3 bonds in the disordered lattice and vibrations of *trans*-polyacetylene chains.[24] A broad and intense band at 1360−1419 cm^{-1} is the main sign of a disordered carbon structure and sp^3-hybridized carbon, which is typically known as D-band in the literature. These results supported the highly intense peak of sp^3 C−H in the ATR-FTIR spectrum as well. Also, the deconvoluted shoulder peak located at 1482 cm^{-1} could be attributed to the vibrations of the sp^2 carbon atoms in a hexagonal lattice graphitic core. The TEM image and the corresponding size distribution of the purified sample (Figure 2E), taken after column chromatography, revealed the spherical-shaped CQDs with an average size of about 4.3 nm and interplanar lattice distances of 0.21−0.23 nm attributed to the (100) planes of the hexagonal phase.

The full-scan spectrum of X-ray photoelectron spectroscopy (XPS) is plotted in Figure 3A, showing three main signals of C 1s (285.1 eV), N 1s (399.5 eV), and O 1s (532.1 eV). It confirms the preparation of oxygen-rich CQDs doped with small amounts of nitrogen. The high-resolution profiles of each element have been included in Figure 3B−D. C 1s is deconvoluted into six distinct component peaks related to the C−H, graphitic C═C, C−C, C−N, C−O, and C═O bonds. The two less intense deconvoluted peaks in the N 1s profile reflect amide (NH) and amine (NH_2) groups. At the same time, the oxygen-rich surface of CQDs was confirmed by the existence of O═C−N, O═C−O, and C−OH contributing signals. It should be noted that Si-related peaks are probably due to the trace amount of Si during the column chromatography process or the silicon wafer substrate used for performing XPS analysis. Based on the ATR-FTIR and XPS measurements, the presence of the main carbon skeleton (C═C, C−C) and functional surface groups of C−O (COO^-), C═O, NH, and NH_2 is demonstrated, leading to a proposed structure of CQDS, as schemed in Figure 1.

As a main physical property of a nanomaterial that determines the capability of being used in LEDs, the optical properties of the purified CQDs were evaluated. Figure 4A shows the UV−vis, PLE, and PL spectra. The absorption

https://doi.org/10.1021/acsanm.3c04915
ACS Appl. Nano Mater. 2024, 7, 2744−2752

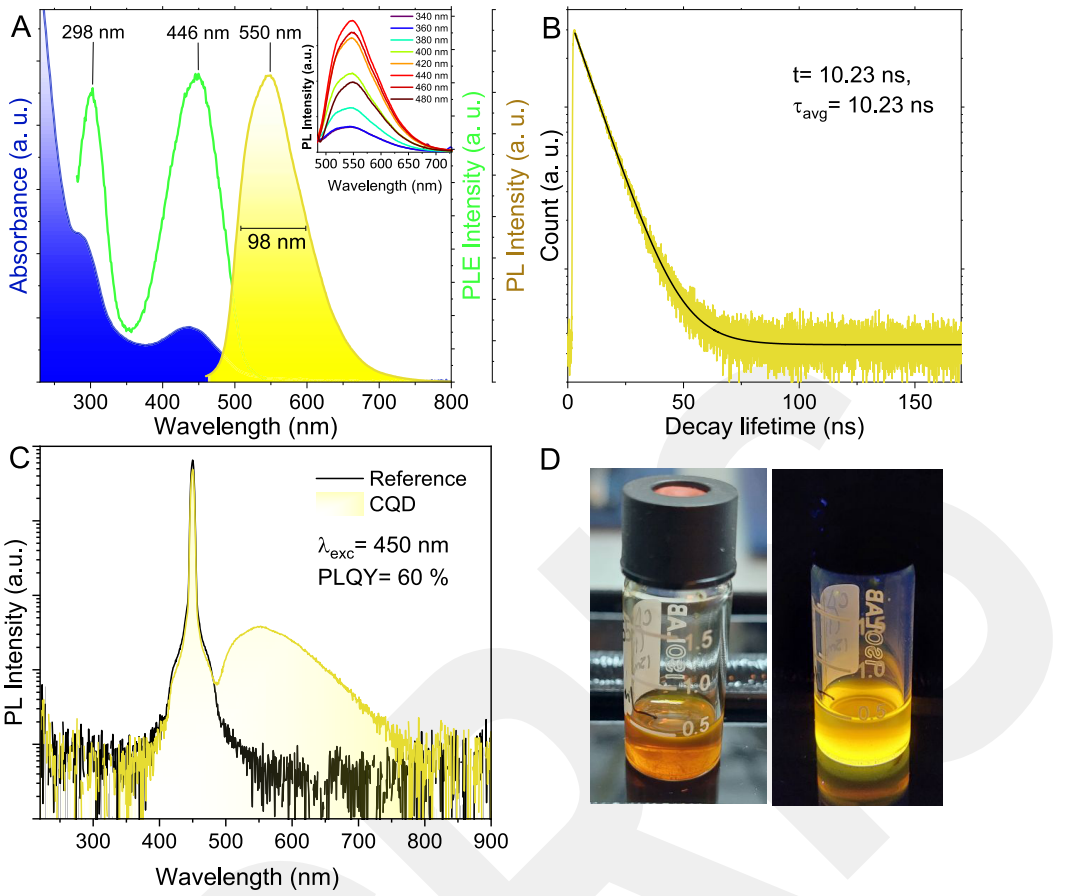

Figure 4. (A) UV−vis, PLE (λ_{ems} = 550 nm), and PL (λ_{exc} = 440 nm) spectra of purified CQDs. The inset shows the excitation-dependent PL spectrum recording from 340 to 480 nm. (B) Logarithmic TRPL profile of the corresponding CQDs obtained at a wavelength of 371 nm. The inset shows the fitting parameters. (C) Absolute PLQY measurement performed using an integrating sphere for yellow-emissive CQDs after column chromatography. (D) Digital images of the purified CQDs, under daylight and 365 nm UV irradiation.

spectrum showed an obvious absorption peak located at 437 nm attributed to the C═O bonds (due to surface C═O functional groups), whose shape is more like that of traditional QDs. On the other hand, a well-known shoulder is distinctive at high energies (wavelengths around 292 nm) due to the $\pi-\pi^*$ transitions of the sp^2 π-conjugated core of the CQDs.[25] Since the energy shift between these two is remarkable, the longer-wavelength absorption can be attributed to the localized defect level[9] or nonbonding orbitals of surface sites.[26] The PLE spectrum also reveals strong excitation signals at 446 and 298 nm, which are in complete accordance with the UV−vis result. To evaluate the emission properties, the PL spectrum was recorded at an excitation wavelength of 440 nm, showing a broad FWHM at 98 nm and a strong signal located at 550 nm. First of all, the peak position shows a very large Stokes shift of more than 100 nm related to the absorption peak, which confirms the determinative role of localized midgap states in optical recombination.[27] On the other hand, the position of the PL spectrum is not dependent on the excitation wavelength (as shown in the inset of Figure 4A), implying the presence of uniform radiative centers. It showed the best emission intensity recorded at an excitation wavelength of 440 nm, as expected from the PLE's longer peak position. It should be noted that during the column chromatography process, blue-emissive products (under a 365 nm UV lamp) were obtained apart from those with yellow emission (Figure 1). To verify the number of energy levels contributing to the recombination process and the average emission lifetime, TRPL measurement was performed (Figure 4B). It demonstrates a decay profile well-matched with a single-exponential pathway and a relatively long lifetime of 10.23 ns, assigned to the midgap radiative recombination centers.[28] This monoexponential behavior also shows a minimal role of trap-contributed recombination and fine uniformity of emissive centers.[29] The PLQY was measured via the comparative method (by choosing Rhodamine 6G with the PL_{peak} located at 560 nm, as the reference dye) for both as-synthesized and purified CQDs, showing a remarkable enhancement from 39 to 54%, respectively, with the approximately similar peak position, as reported elsewhere.[30] To confirm our measurement, the PLQY was double-checked with the integrated measurement system, showing a PLQY of 60% at an excitation wavelength of 450 nm (Figure 4C). This high PLQY can be attributed to efficient electronic transitions in the conjugated aromatic rings and proper passivation of nonradiative surface traps (supported by the monoexponential TRPL profile of CQDs). Besides, urea introduces nitrogen to the structure of CQDs creating nitrogen-related radiative centers, which resulted in CQDs with bright yellow emission. To demonstrate the noticeable role of urea as a nitrogen source, the same synthesis recipe was used without employing urea. As plotted in Figure S1, the urea-free samples showed very different optical properties. First of all, the obvious absorption peak of yellow-emissive CQDs located at 446 nm disappeared. Second, the PL emission measurements con-

https://doi.org/10.1021/acsanm.3c04915
ACS Appl. Nano Mater. 2024, 7, 2744−2752

Table 1. Optical Emission Characteristics of the Purified CQDs and Comparison of Their Results with Recent Reports

references/year of pub.	PL position (nm)	FWHM (nm)	PLQY (%)	decay characteristics average emission lifetime (ns)	application	refs
Jiang et al. 2015	568	>100	32	biexponential, 1.87	sensing and cellular imaging	31
Ke et al. 2016	523	>150	2	biexponential, 1.98	bioimaging	32
Wu et al. 2018	560	~100	6	—	Ion sensor	33
Zheng et al. 2020	562	75	53	—	color conversion WLED	34
Ding et al. 2020	600	>120	16.7	biexponential, 3.51	electroluminescent device	35
present study 2023	550	98	60	monoexponential, 10.23	electroluminescent WLED	—

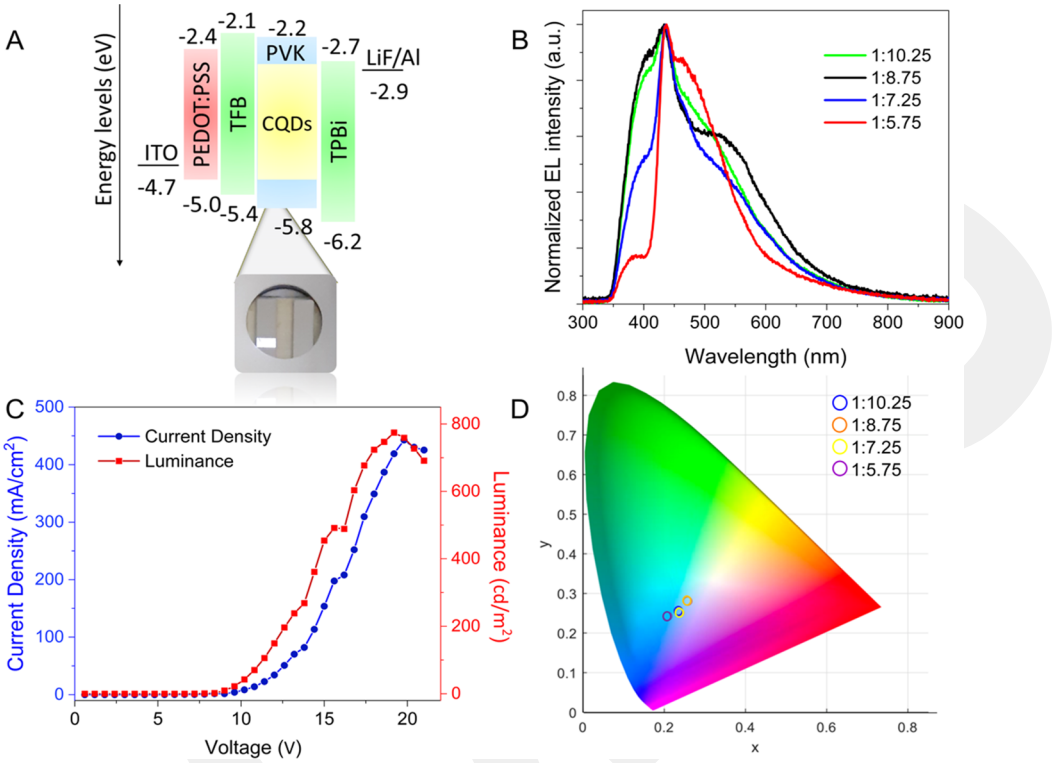

Figure 5. (A) Energy level diagram of the CQD-LED with the inset of a photograph of the device at a driving voltage of 14.4 V and device structure. (B) Normalized EL spectra of the CQD-LEDs at different CQD:PVK ratios. (C) *J*–*V*–*L* characteristic curve of the CQD-LED (with a volume ratio of 1:10.25). (D) CIE coordinates of the CQD-LEDs fabricated at different CQD:PVK ratios at the driving voltage of 14.4 V.

firmed an excitation-dependent emission at 470 nm (λ_{exc} = 375 and 507 nm) (λ_{exc} = 430 nm), which has experienced an obvious blue shift, completely different from the optical properties of urea-included yellow-emissive CQDs (with excitation-independent emission at 550 nm under λ_{exc} = 440 nm). Even the calculated PLQY of the urea-free samples quenched to 12%. Therefore, urea introduces new radiative centers, which improves the PL emission properties of the prepared sample. By evaluating the effect of molecular weight on the optical properties of the similar CQD structure, Guo et al. showed that PL characteristics are related to the size of CQDs, which is normally observed in conventional QDs.[8] Direct images of the purified CQDs under daylight and a 365 nm UV lamp are provided in Figure 4D, emphasizing the bright yellow emission. Table 1 summarizes the PL emission features of the purified CQDs and compares them with other reports in the field confirming the luminescent merits of the prepared CQDs. For any practical application, the PL emission should be stable with long-time durability against harsh conditions. In an electroluminescent device, stability against elevated temperature and UV irradiation is more important. In this regard, the purified CQDs were subjected to 365 nm UV irradiation (2 cm distance from the UV source), and their PL emission spectrum was recorded at different time intervals (Figure S2A). It showed that even after 100 min, the PL emission intensity drops slightly. The PL emission spectrum of the purified CQDs was also recorded for heated-up samples from room temperature to 95 °C (Figure S2B). Again, it showed remarkable stability of emission in such a way that 94% of the initial emission is preserved. Besides, the PL, PLE, and UV–vis spectroscopies of the purified CQDs were evaluated after 14 months of storage at 4 °C to evaluate their lifetime (Figure S3). As demonstrated, there is no change in the optical spectra after 14 months of storage of purified CQDs. The PLQY measurement after this time duration also confirmed the value of 55.2% using the comparative method (with Rhodamine 6G as the reference dye). Both of them prove the excellent stability of the prepared sample over time. Such a durability performance is probably due to the surface termination of CQDs by long-chain *n*-octylamine molecules, which work as an efficient extra shell layer. This also reduces the possibility of nanoparticle agglomeration via an increase in the steric distance of the carbonized nanoparticles.

https://doi.org/10.1021/acsanm.3c04915
ACS Appl. Nano Mater. 2024, 7, 2744–2752

Table 2. Comparison of the Previous Studies that Have Used a CQD:PVK Mixture as the Light-Emitting Layer (Driving Voltage is 14.4 V) with the Present Study

device structure	color	V_{on} (V)	L_{max} (cd·m^{-2})	EQE (%)	CIE (x,y)	refs
ITO/PVK:CQDs/TPBI or TmPyPB/LiF/Al	white	∼8	339.5	—	0.41, 0.48	15
ITO/PEDOT:PSS/PVK:CQDs/TPBi/Ca/Al	multi	3.5	1882−4762	—		39
ITO/PEDOT:PSS/PVK:HCP-DB-CQDs/TPBi/Ca/Al	blue	5−8	5240	4	0.15, 0.05	29
ITO/PEDOT:PSS/PVK:CQDs/TPBI/Liq/Al	blue	6.7	648	2.1	0.14, 0.10	41
ITO/PEDOT:PSS/PVK:CQDs/TPBI/Liq/Al	white	3.6	626	1.18	0.33, 0.33	38
ITO/PEDOT:PSS/PVK:Y-CQDs/TPBI/LiF/Al	white	4.0	1718	0.004−0.18	0.48, 0.42	42
ITO/PEDOT:PSS/TFB/PVK:CQDs/TPBI/Liq/Al	green		681	0.18	0.35, 0.53	43
ITO/PEDOT:PSS/TFB/PVK:CQDs/TPBI/Liq/Al	yellow-green	9.9	220	0.18	0.30, 0.65	35
ITO/PEDOT:PSS/PVK:CQDs/TPBI/Liq/Al	blue	8.17	176	—	0.17, 0.10	44
ITO/PEDOT:PSS/TFB/PVK:CQDs/TPBI/LiF/Al	white	8.4[a]	774.3	0.35	0.23, 0.26	present study
		9	223.6	0.28	0.26, 0.28	
		8.4	267.3	0.23	0.24, 0.25	
		6	391.8	0.76	0.21, 0.24	

[a]From top to bottom, the CQD:PVK ratios in the present work are 1:10.25, 1:8.75, 1:7.25, and 1:5.75, respectively.

While showing a broad PL signal with a large FWHM value is not generally attractive for optoelectronic purposes, due to the coverage of almost all of the visible spectrum, it is becoming a unique property of CQDs to directly reach a high-performance WLED. In this case, an organic semiconductor is introduced as the host material to avoid $\pi-\pi$ stacking of carbon dots in the solid film form.[16,36,37] Due to its large band gap and neat film-forming properties, the host−guest blend of CQD-doped PVK is used as an emission layer (EML) to fabricate CQD-LEDs to further evaluate the electroluminescent properties. The device configuration is shown as an inset in Figure 5A, and it comprises, from up to bottom, the layers of the aluminum (Al) cathode, lithium fluoride (LiF) electron buffer layer, 1,3,5-*tris*(*N*-phenylbenzimidazol-2-yl)benzene (TPBi) electron transport layer, PVK:CQD emitting layer, TFB hole transport layer, PEDOT:PSS hole injection layer, and indium−tin oxide (ITO) anode. The highest occupied molecular orbital (HOMO) energy levels of ITO and PEDOT:PSS are very close to each other. This allows the carriers to pass through the barrier to reach charge balance. The same is true for the lowest unoccupied molecular orbital (LUMO) energy levels between Al/LiF and TPBi, so this helps charge balance, too. Since the energy levels of CQDs are located within the energy levels of PVK, the transferred electrons and holes can undergo radiative recombination in CQDs to produce electroluminescence.[35,38] The energy levels of the HOMO and LUMO of the CQD:PVK blend were obtained from literatures.[39,40] In sandwich-structured LEDs, a CQD-PVK film served as the emissive layer. Due to fluorescence quenching caused by CQD aggregation, pure CQDs as the light-emitting layer often cannot create high-purity CD-LEDs. PVK acts as a host platform for CQDs. As a result, doping CQDs into PVK as an electron transport layer significantly suppresses the luminescence quenching of CQD-LEDs. The energy level schematic shown in Figure 5A is used to describe how the functional layers interact. Figure 5B shows the normalized EL spectra of the CQD-LEDs, fabricated with different volume ratios of CQDs in PVK solution at different driving voltages where the maximum luminescence occurs. The spectra of the CQD-LEDs prepared with different volume ratios will change accordingly, but in all cases, there are various peaks (shoulders) related to PVK and CQDs. Depending on the CQD:PVK ratio, the main emission peak of the EL spectra is located around 433−437 nm, and this blue emission originates from PVK, while the second one which is located at around 550 nm originated from the CQDs. It was found that this peak originates from CQDs rather than the exciplex of PVK and TPBi due to complex emission of the interface between the hole transport layer and the electron transport layer. Furthermore, by a change in the volume ratio of CQD-to-PVK, the intensity ratio of these differentiated peaks also changes due to the partial exciton transfer and electroluminescence from both CQDs and PVK.

The current density−voltage−luminance ($J-V-L$) characteristics of the CQD-LED (with a volume ratio of 1:10.25) that has the highest luminance are given in Figure 5C. The current density and the luminance increase under a driving voltage of 9.0−21.0 V, and the maximum luminance and EQE of 774.3 cd·m^{-2} and 0.76%, respectively, were achieved at a driving voltage of 19.2 V, with the CIE coordinates of (0.23, 0.26). Figure S4A,B shows the $J-V$ and $L-V$ characteristics of CQD-LEDs for all devices, respectively. When compared with other devices, the 1:10.25 volume ratio showed a higher luminescence and current density values. Ultimately, the CIE coordinates of CQD-LEDs with different volume ratios are calculated, which are presented in Figure 5D. When the volume ratios of CQD:PVK are 1:10.25, 1:8.75, 1:7.25, and 1:5.75, the relevant CIE coordinates are situated at (0.23, 0.26), (0.26, 0.28), (0.24, 0.25), and (0.21, 0.24), respectively, which shows that by changing the volume ratio of the CQD in PVK solution, the color of the devices can be modified. To compare the presented electroluminescent results in this study with the reported literature, Table 2 has been included, indicating good results for WLEDs fabricated by the CQDs.

4. CONCLUSIONS

In this work, yellow-emissive CQDs with a PLQY of 60% were synthesized through a solvothermal method followed by column chromatography-assisted purification. The tiny purified samples with an average size of 4.5 nm showed an excitation wavelength-independent PL peak position with a monoexponential TRPL profile of 10.23 ns, showing the optical merits of the prepared samples. CQDs are suitable for solution-processed device applications, and PVK is introduced as a host to reduce the aggregation problem of CQDs in their solid-state form. By adjustment of the volume ratio between CQD and PVK, a shift in CIE $x-y$ coordinates from 0.23−0.26 to 0.21−0.24 is realized. As the volume ratio of CQD:PVK

https://doi.org/10.1021/acsanm.3c04915
ACS Appl. Nano Mater. 2024, 7, 2744−2752

solution changes from 1:5.75 to 1:8.75, the CIE coordinate shifts from the blue region to the white region. While L_{max} values for CQD-LEDs vary between 223.6 and 774.3 cd·m^{-2}, EQE values range between 0.23 and 0.76%. These results pave the way for the systematic engineering of white light using CQDs.

■ ASSOCIATED CONTENT

Supporting Information

The Supporting Information is available free of charge at https://pubs.acs.org/doi/10.1021/acsanm.3c04915.

PL and UV−vis spectra of the CQDs prepared without urea; PL stability of purified CQDs against UV irradiation, temperature, and time; and the current density and luminance versus voltage characteristic curves of WLEDs (PDF)

■ AUTHOR INFORMATION

Corresponding Authors

Ehsan Soheyli − *Department of Electrical-Electronics Engineering, Abdullah Gul University, Kayseri 38080, Türkiye;* Present Address: Department of Physics, Faculty of Science, Ilam University, Ilam, 69315-516 Iran; orcid.org/0000-0002-1403-7934; Email: ehsan.soheyli@agu.edu.tr

Evren Mutlugun − *Department of Electrical-Electronics Engineering, Abdullah Gul University, Kayseri 38080, Türkiye; UNAM—Institute of Materials Science and Nanotechnology, Bilkent University, Ankara 06800, Türkiye;* orcid.org/0000-0003-3715-5594; Email: evren.mutlugun@agu.edu.tr

Authors

Kevser Sahin Tiras − *Department of Physics, Faculty of Sciences, Erciyes University, Kayseri 38030, Türkiye*

Aysenur Biçer − *Department of Electrical-Electronics Engineering, Abdullah Gul University, Kayseri 38080, Türkiye;* Present Address: Department of Electrical and Electronics Engineering, Faculty of Engineering, Middle East Technical University, Ankara, Türkiye

Complete contact information is available at: https://pubs.acs.org/10.1021/acsanm.3c04915

Author Contributions

K.S.T.: investigation, data curation, and writing—original draft. A.B.: investigation and validation. E.S.: investigation, conceptualization, data curation, methodology, validation, writing—original draft, and writing—review and editing. E.M.: conceptualization, validation, funding acquisition, project administration, resources, and writing—review and editing.

Notes

The authors declare no competing financial interest.

■ ACKNOWLEDGMENTS

The authors would like to acknowledge the TUBITAK 20AG026 Project.

■ REFERENCES

(1) Xu, Q.; Niu, Y.; Li, J.; Yang, Z.; Gao, J.; Ding, L.; Ni, H.; Zhu, P.; Liu, Y.; Tang, Y.; Lv, Z.-P.; Peng, B.; Hu, T. S.; Zhou, H.; Xu, C. Recent Progress of Quantum Dots for Energy Storage Applications. *Carbon Neutrality* **2022**, *1* (1), No. 13.

(2) Shen, C.-L.; Lou, Q.; Liu, K.-K.; Dong, L.; Shan, C.-X. Chemiluminescent Carbon Dots: Synthesis, Properties, and Applications. *Nano Today* **2020**, *35*, No. 100954.

(3) Savaedi, S.; Soheyli, E.; Zheng, G.; Lou, Q.; Sahraei, R.; Shan, C. Excitation-Independent Deep-Blue Emitting Carbon Dots with 62% Emission Quantum Efficiency and Monoexponential Decay Profile for High-Resolution Fingerprint Identification. *Nanotechnology* **2022**, *33* (44), No. 445601.

(4) Zhu, P.; Liu, Y.; Tang, Y.; Zhu, S.; Liu, X.; Yin, L.; Liu, Q.; Yu, Z.; Xu, Q.; Luo, D.; Wang, J. Bi-Doped Carbon Quantum Dots Functionalized Liposomes with Fluorescence Visualization Imaging for Tumor Diagnosis and Treatment. *Chin. Chem. Lett.* **2023**, No. 108689.

(5) Wang, B.; Cai, H.; Waterhouse, G. I. N.; Qu, X.; Yang, B.; Lu, S. Carbon Dots in Bioimaging, Biosensing and Therapeutics: A Comprehensive Review. *Small Sci.* **2022**, *2* (6), No. 2200012.

(6) Shi, Y.; Wang, Z.; Meng, T.; Yuan, T.; Ni, R.; Li, Y.; Li, X.; Zhang, Y.; Tan, Z.; Lei, S.; Fan, L. Red Phosphorescent Carbon Quantum Dot Organic Framework-Based Electroluminescent Light-Emitting Diodes Exceeding 5\% External Quantum Efficiency. *J. Am. Chem. Soc.* **2021**, *143* (45), 18941−18951.

(7) Wang, Y.; Chang, Q.; Xue, C.; Yang, J.; Hu, S. Chemical Treatment of Biomasswastes as Carbon Dot Carriers for Solar-Driven Water Purification. *J. Colloid Interface Sci.* **2022**, *621*, 33−40.

(8) Guo, J.; Lu, Y.; Xie, A.-Q.; Li, G.; Liang, Z.-B.; Wang, C.-F.; Yang, X.; Chen, S. Yellow-Emissive Carbon Dots with High Solid-State Photoluminescence. *Adv. Funct. Mater.* **2022**, *32* (20), No. 2110393.

(9) Zheng, G.; Wang, T.; Lou, Q.; Shen, C.; Wu, M.; Sun, J.; Ji, W.; Zang, J.; Liu, K.; Dong, L.; Shan, C. Localized Excitonic Electroluminescence from Carbon Nanodots. *J. Phys. Chem. Lett.* **2022**, *13* (6), 1587−1595.

(10) Ma, J.; Zhang, L.; Chen, X.; Su, R.; Shi, Q.; Zhao, S.; Xu, Q.; Xu, C. Mass Production of Highly Fluorescent Full Color Carbon Dots from the Petroleum Coke. *Chin. Chem. Lett.* **2021**, *32* (4), 1532−1536.

(11) Wei, C.; Hu, S.; Liang, F.; Song, Z.; Liu, X. One-Pot Synthesis of Concentration and Excitation Dual-Dependency Truly Full-Color Photoluminescence Carbon Dots. *Chin. Chem. Lett.* **2022**, *33* (8), 4116−4120.

(12) Zhang, D.; Chao, D.; Yu, C.; Zhu, Q.; Zhou, S.; Tian, L.; Zhou, L. One-Step Green Solvothermal Synthesis of Full-Color Carbon Quantum Dots Based on a Doping Strategy. *J. Phys. Chem. Lett.* **2021**, *12* (37), 8939−8946.

(13) Zhang, X.; Zeng, L.; Sun, T.; Xue, X.; Wei, B. Facilely Synthesized Carbon Dots and Configurated Light-Emitting Diodes with Efficient Electroluminescence. *Phys. Chem. Chem. Phys.* **2022**, *24* (43), 26511−26518.

(14) Wang, J.; Zhang, F.; Wang, Y.; Yang, Y.; Liu, X. Efficient Resistance against Solid-State Quenching of Carbon Dots towards White Light Emitting Diodes by Physical Embedding into Silica. *Carbon* **2018**, *126*, 426−436.

(15) Xu, J.; Miao, Y.; Zheng, J.; Wang, H.; Yang, Y.; Liu, X. Carbon Dot-Based White and Yellow Electroluminescent Light Emitting Diodes with a Record-Breaking Brightness. *Nanoscale* **2018**, *10* (23), 11211−11221.

(16) Yuan, F.; Wang, Z.; Li, X.; Li, Y.; Tan, Z.; Fan, L.; Yang, S. Bright Multicolor Bandgap Fluorescent Carbon Quantum Dots for Electroluminescent Light-Emitting Diodes. *Adv. Mater.* **2017**, *29* (3), No. 1604436.

(17) Xu, J.; Miao, Y.; Zheng, J.; Yang, Y.; Liu, X. Ultrahigh Brightness Carbon Dot−Based Blue Electroluminescent LEDs by Host−Guest Energy Transfer Emission Mechanism. *Adv. Opt. Mater.* **2018**, *6* (14), No. 1800181.

(18) Wang, L.; Li, W.; Yin, L.; Liu, Y.; Guo, H.; Lai, J.; Han, Y.; Li, G.; Li, M.; Zhang, J.; Vajtai, R.; Ajayan, P. M.; Wu, M. Full-Color Fluorescent Carbon Quantum Dots. *Sci. Adv.* **2020**, *6* (40), No. eabb6772.

(19) Gude, V.; Das, A.; Chatterjee, T.; Mandal, P. K. Molecular Origin of Photoluminescence of Carbon Dots: Aggregation-Induced Orange-Red Emission. *Phys. Chem. Chem. Phys.* **2016**, *18* (40), 28274−28280.
(20) Zhu, J.; Shao, H.; Bai, X.; Zhai, Y.; Zhu, Y.; Chen, X.; Pan, G.; Dong, B.; Xu, L.; Zhang, H.; Song, H. Modulation of the Photoluminescence in Carbon Dots through Surface Modification: From Mechanism to White Light-Emitting Diodes. *Nanotechnology* **2018**, *29* (24), No. 245702.
(21) Zhi, B.; Yao, X.; Wu, M.; Mensch, A.; Cui, Y.; Deng, J.; Duchimaza-Heredia, J. J.; Trerayapiwat, K. J.; Niehaus, T.; Nishimoto, Y.; Frank, B. P.; Zhang, Y.; Lewis, R. E.; Kappel, E. A.; Hamers, R. J.; Fairbrother, H. D.; Orr, G.; Murphy, C. J.; Cui, Q.; Haynes, C. L. Multicolor Polymeric Carbon Dots: Synthesis, Separation and Polyamide-Supported Molecular Fluorescence. *Chem. Sci.* **2021**, *12* (7), 2441−2455.
(22) Lou, Q.; Ni, Q.; Niu, C.; Wei, J.; Zhang, Z.; Shen, W.; Shen, C.; Qin, C.; Zheng, G.; Liu, K.; Zang, J.; Dong, L.; Shan, C.-X. Carbon Nanodots with Nearly Unity Fluorescent Efficiency Realized via Localized Excitons. *Adv. Sci.* **2022**, *9* (30), No. 2203622.
(23) Shen, C.-L.; Lou, Q.; Liu, K.-K.; Zheng, G.-S.; Song, R.-W.; Zang, J.-H.; Dong, L.; Shan, C.-X. Supramolecular Self-Assembly of Carbon Nanodots through Edge Functionalized Interaction. *Carbon* **2023**, *213*, No. 118217.
(24) Stepanidenko, E. A.; Skurlov, I. D.; Khavlyuk, P. D.; Onishchuk, D. A.; Koroleva, A. V.; Zhizhin, E. V.; Arefina, I. A.; Kurdyukov, D. A.; Eurov, D. A.; Golubev, V. G.; Baranov, A. V.; Fedorov, A. V.; Ushakova, E. V.; Rogach, A. L. Carbon Dots with an Emission in the Near Infrared Produced from Organic Dyes in Porous Silica Microsphere Templates. *Nanomaterials* **2022**, *12* (3), No. 543, DOI: 10.3390/nano12030543.
(25) Li, T.; Shi, W.; Mao, Q.; Chen, X. Regulating the Photoluminescence of Carbon Dots via a Green Fluorine-Doping-Derived Surface-State-Controlling Strategy. *J. Mater. Chem. C* **2021**, *9* (48), 17357−17364.
(26) Joseph, J.; Anappara, A. A. Cool White, Persistent Room-Temperature Phosphorescence in Carbon Dots Embedded in a Silica Gel Matrix. *Phys. Chem. Chem. Phys.* **2017**, *19* (23), 15137−15144.
(27) Yan, F.; Sun, Z.; Zhang, H.; Sun, X.; Jiang, Y.; Bai, Z. The Fluorescence Mechanism of Carbon Dots, and Methods for Tuning Their Emission Color: A Review. *Microchim. Acta* **2019**, *186* (8), No. 583.
(28) Chen, Y.; Lian, H.; Wei, Y.; He, X.; Chen, Y.; Wang, B.; Zeng, Q.; Lin, J. Concentration-Induced Multi-Colored Emissions in Carbon Dots: Origination from Triple Fluorescent Centers. *Nanoscale* **2018**, *10* (14), 6734−6743.
(29) Yuan, F.; Wang, Y. K.; Sharma, G.; Dong, Y.; Zheng, X.; Li, P.; Johnston, A.; Bappi, G.; Fan, J. Z.; Kung, H.; Chen, B.; Saidaminov, M. I.; Singh, K.; Voznyy, O.; Bakr, O. M.; Lu, Z. H.; Sargent, E. H. Bright High-Colour-Purity Deep-Blue Carbon Dot Light-Emitting Diodes via Efficient Edge Amination. *Nat. Photonics* **2020**, *14* (3), 171−176.
(30) Sato, K.; Katakami, R.; Iso, Y.; Isobe, T. Surface-Modified Carbon Dots with Improved Photoluminescence Quantum Yield for Color Conversion in White-Light-Emitting Diodes. *ACS Appl. Nano Mater.* **2022**, *5* (6), 7664−7669.
(31) Jiang, K.; Sun, S.; Zhang, L.; Wang, Y.; Cai, C.; Lin, H. Bright-Yellow-Emissive N-Doped Carbon Dots: Preparation, Cellular Imaging, and Bifunctional Sensing. *ACS Appl. Mater. Interfaces* **2015**, *7* (41), 23231−23238.
(32) Ke, C.-C.; Yang, Y.-C.; Tseng, W.-L. Synthesis of Blue-, Green-, Yellow-, and Red-Emitting Graphene-Quantum-Dot-Based Nanomaterials with Excitation-Independent Emission. *Part. Part. Syst. Charact.* **2016**, *33* (3), 132−139.
(33) Wu, Q.; Wang, X.; Rasaki, S. A.; Thomas, T.; Wang, C.; Zhang, C.; Yang, M. Yellow-Emitting Carbon-Dots-Impregnated Carboxy Methyl Cellulose/Poly-Vinyl-Alcohol and Chitosan: Stable, Free-standing, Enhanced-Quenching Cu2+ Ions Sensor. *J. Mater. Chem. C* **2018**, *6* (16), 4508−4515.
(34) Zheng, K.; Li, X.; Chen, M.; Gong, Y.; Tang, A.; Wang, Z.; Wei, Z.; Guan, L.; Teng, F. Controllable Synthesis Highly Efficient Red, Yellow and Blue Carbon Nanodots for Photo-Luminescent Light-Emitting Devices. *Chem. Eng. J.* **2020**, *380*, No. 122503.
(35) Ding, Y.; Li, X.; Zheng, Z.; Chen, M.; Zhang, Y.; Liu, Z.; Wang, F.; Guan, L. Preparation and Luminescent Modulation of Yellow Carbon Dots for Electroluminescent Device. *J. Lumin.* **2022**, *249*, No. 119036.
(36) Jia, H.; Wang, Z.; Yuan, T.; Yuan, F.; Li, X.; Li, Y.; Tan, Z.; Fan, L.; Yang, S. Electroluminescent Warm White Light-Emitting Diodes Based on Passivation Enabled Bright Red Bandgap Emission Carbon Quantum Dots. *Adv. Sci.* **2019**, *6* (13), No. 1900397.
(37) Kwon, W.; Kim, Y.-H.; Lee, C.-L.; Lee, M.; Choi, H. C.; Lee, T.-W.; Rhee, S.-W. Electroluminescence from Graphene Quantum Dots Prepared by Amidative Cutting of Tattered Graphite. *Nano Lett.* **2014**, *14* (3), 1306−1311.
(38) Wang, X.; Wang, B.; Wang, H.; Zhang, T.; Qi, H.; Wu, Z.; Ma, Y.; Huang, H.; Shao, M.; Liu, Y.; Li, Y.; Kang, Z. Carbon-Dot-Based White-Light-Emitting Diodes with Adjustable Correlated Color Temperature Guided by Machine Learning. *Angew. Chem., Int. Ed.* **2021**, *60* (22), 12585−12590.
(39) Yuan, F.; Yuan, T.; Sui, L.; Wang, Z.; Xi, Z.; Li, Y.; Li, X.; Fan, L.; Tan, Z.; Chen, A.; Jin, M.; Yang, S. Engineering Triangular Carbon Quantum Dots with Unprecedented Narrow Bandwidth Emission for Multicolored LEDs. *Nat. Commun.* **2018**, *9* (1), No. 2249.
(40) Kim, J. K.; Bae, S.; Yi, Y.; Park, M. J.; Kim, S. J.; Myoung, N.; Lee, C.-L.; Hong, B. H.; Park, J. H. Origin of White Electroluminescence in Graphene Quantum Dots Embedded Host/Guest Polymer Light Emitting Diodes. *Sci. Rep.* **2015**, *5* (1), No. 11032, DOI: 10.1038/srep11032.
(41) Wang, X.; Ma, Y.; Wu, Q.; Wang, Z.; Tao, Y.; Zhao, Y.; Wang, B.; Cao, J.; Wang, H.; Gu, X.; Huang, H.; Li, S.; Wang, X.; Hu, F.; Shao, M.; Liao, L.; Sham, T.-K.; Liu, Y.; Kang, Z. Ultra-Bright and Stable Pure Blue Light-Emitting Diode from O, N Co-Doped Carbon Dots. *Laser Photonics Rev.* **2021**, *15* (3), No. 2000412.
(42) Wang, Z.; Jiang, N.; Liu, M.; Zhang, R.; Huang, F.; Chen, D. Bright Electroluminescent White-Light-Emitting Diodes Based on Carbon Dots with Tunable Correlated Color Temperature Enabled by Aggregation. *Small* **2021**, *17* (52), No. 2104551.
(43) Zheng, Z.; Liu, Z.; Ding, Y.; Chen, M.; Lv, P.; Tang, A.; Wang, F.; Guan, L.; Li, X.; Liang, B. Structural Engineering toward High Monochromaticity of Carbon Dots-Based Light-Emitting Diodes. *J. Phys. Chem. Lett.* **2021**, *12* (50), 12107−12113.
(44) Zhang, T.; Wang, X.; Wu, Z.; Yang, T.; Wang, J.; Zhao, H.; Huang, H.; Liu, Y.; Kang, Z. Carbon Dots Promote the Carrier Recombination in Poly (9-Vinyl Carbazole) to Enhance Its Electroluminescence. *Appl. Surf. Sci.* **2022**, *585*, No. 152649.

https://doi.org/10.1021/acsanm.3c04915
ACS Appl. Nano Mater. 2024, 7, 2744−2752